

Multimetallic Permethylpentalene Hydride Complexes

Duncan A. X. Fraser, Zoë R. Turner, Robert T. Cooper, Jean-Charles Buffet, Jennifer C. Green,* and Dermot O'Hare*

Cite This: *Inorg. Chem.* 2022, 61, 12207–12218

Read Online

ACCESS |



Metrics & More

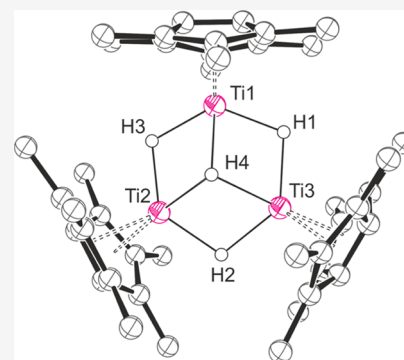


Article Recommendations



Supporting Information

ABSTRACT: The synthesis and characterization of group 4 permethylpentalene ($\text{Pn}^* = \text{C}_8\text{Me}_6$) hydride complexes are explored; in all cases, multimetallic hydride clusters were obtained. Group 4 lithium metal hydride clusters were obtained when reacting the metal dihalides with hydride transfer reagents such as LiAlH_4 , and these species featured an unusual hexagonal bipyramidal structural motif. Only the zirconium analogue was found to undergo hydride exchange in the presence of deuterium. In contrast, a trimetallic titanium hydride cluster was isolated on reaction of the titanium dialkyl with hydrogen. This diamagnetic, mixed valence species was characterized in the solid state, as well as by solution electron paramagnetic resonance and nuclear magnetic resonance spectroscopy. The structure was further probed and corroborated by density functional theory calculations, which illustrated the formation of a metal-cluster bonding orbital responsible for the diamagnetism of the complex. These permethylpentalene hydride complexes have divergent structural motifs and reactivity in comparison with related classical cyclopentadienyl analogues.



INTRODUCTION

Transition metal hydride complexes play a key role in the addition of hydrogen to unsaturated substrates, one of the most common chemical transformations employed in the production of commodity and fine chemicals alike.¹ The ability of metal hydrides to overcome kinetic barriers to hydrogen transfer has encouraged widespread investigation into their fundamental organometallic chemistry² and role in homogeneous catalysis.³

Group 4 metal hydride complexes, typically metallocene hydrides,⁴ have been extensively explored and demonstrate a wide range of uses in the hydrogenation of olefinic bonds,⁵ polymerization catalysis,⁶ and the reduction of carbon oxides,⁷ as well as playing a role in understanding activation of dinitrogen.⁸ Notably, Schwartz's reagent ($\text{Cp}_2\text{Zr}(\text{H})\text{Cl}$) has proved to be a powerful tool in organic synthesis, allowing for hydrozirconation and subsequent chemoselective C–C, C–N, and C–X bond formation with good functional group tolerance.⁹ Related polyhydride complexes not only possess interesting structural motifs but have also shown to demonstrate remarkable power in activating challenging bonds;¹⁰ Hou and co-workers have reported both dinitrogen reduction and cleavage^{10c} and C–C activation of benzene^{10b} by the trimetallic heptahydride cluster $\{(\eta^5\text{-C}_5\text{Me}_4\text{SiMe}_3)\text{-Ti}\}_3(\mu_3\text{-H})(\mu_2\text{-H})_6$. Noncyclopentadienyl-supported group 4 metal hydrides are comparatively rarer;¹¹ Okuda and co-workers have reported the preparation of $[\{\text{Zr}(\text{Me}_3\text{TACD})(\mu\text{-H})_2\}_2][\text{A}]_2$ ($\text{Me}_3\text{TACD} = 1,4,7\text{-trimethyl-1,4,7,10-tetraazacyclododecane}$; $\text{A} = \text{Al}\{\text{OC}(\text{CF}_3)_3\}_4$, $\text{B}\{3,5\text{-C}_6\text{H}_3(\text{CF}_3)_2\}_4$, $\text{B}\{3,5\text{-C}_6\text{H}_3\text{Cl}_2\}_4$, and BPh_4) by hydrogenolysis (50 bar H_2)

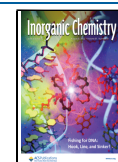
of the corresponding neosilyl complexes.^{11a} Related hydrogenolysis with P_2N_2 Hf methyl complexes, $\{\text{PhP}(\text{CH}_2\text{SiMe}_2\text{NSiMe}_2\text{CH}_2)_2\text{PPh}\}\text{HfMe}_2$, reported by Fryzuk and co-workers, also afforded binuclear tetrahydride complexes.^{11e}

There are a number of synthetic strategies used to access metal-hydride complexes. With reduced metal complexes, oxidative addition of H_2 provides an atom economical route to install hydride ligands,^{7a,12} or alternatively alkyl, benzyl, or aryl derivatives can undergo σ -bond metathesis, which proceeds with loss of the protonated ligand.¹³ With metal-halide complexes, hydride transfer reagents can be employed,^{4a,c,14} which provide a useful lever to control the reaction outcome by tuning the hydride donor capacity of the H^- source.¹⁵ Less commonly, reaction of metal-halide complexes with alkylating agents bearing β -hydrogens can allow for the synthesis of metal-hydride complexes following elimination.¹⁶

Herein, we describe two new group 4 lithium multimetallic hydride complexes, which are synthesized by the reaction of hydride transfer reagents and permethylpentalene ($\text{Pn}^* = \text{C}_8\text{Me}_6$) metal-chloride precursors. In addition, the trimetallic titanium complex $\text{Pn}^*\text{Ti}_3(\mu_2\text{-H})_3(\mu_3\text{-H})$ is isolated and its

Received: April 19, 2022

Published: July 25, 2022

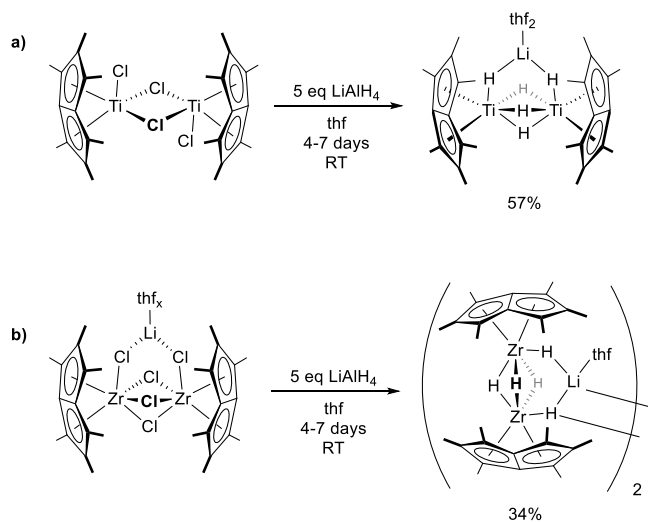


structure and bonding are investigated through spectroscopic studies as well as density functional theory calculations.

RESULTS AND DISCUSSION

Synthesis of Group 4 Lithium Metal Hydride Clusters: $\text{Pn}^*\text{M}_2(\mu_2\text{-H})_5\text{Li.thf}_x$. The reactivity of $(\text{Pn}^*\text{TiCl})_2(\mu\text{-Cl})_2$ with a variety of hydride transfer reagents was investigated. LiH, KH, and NaBH_4 all displayed no reactivity in polar and nonpolar solvents at both ambient and elevated temperatures. By contrast LiAlH_4 in thf was observed to successfully form hydride derivatives, consuming the starting material and forming a number of new hydridic resonances in proton nuclear magnetic resonance (^1H NMR) spectra <0 ppm. Despite repeated attempts, variation of the reaction conditions did not allow for the clean isolation of these intermediate-hydride species. However, allowing the reaction to proceed for 7 days with 5 equiv of LiAlH_4 led to the eventual formation of a single product observed spectroscopically, $\text{Pn}^*\text{Ti}_2(\mu_2\text{-H})_5\text{Li.thf}_x$ (Scheme 1). Bulk synthesis was achieved by the

Scheme 1. Synthesis of (a) $\text{Pn}^*\text{Ti}_2(\mu_2\text{-H})_5\text{Li.thf}_2$ and (b) $[\text{Pn}^*\text{Zr}_2(\mu_2\text{-H})_4(\mu_3\text{-H})\text{Li.thf}]_2$



reaction of $(\text{Pn}^*\text{TiCl})_2(\mu\text{-Cl})_2$ and 5 equiv of LiAlH_4 in thf over 4 to 7 days. Subsequent crystallization from thf afforded yellow crystals of $\text{Pn}^*\text{Ti}_2(\mu_2\text{-H})_5\text{Li.thf}_x$ in 57% yield ($x = 0.9$).

The ^1H NMR spectrum, in $\text{C}_4\text{D}_8\text{O}$, displays 3 $\text{Pn}^*\text{-Me}$ resonances of relative integration 12:12:12, indicating the presence of a time-averaged mirror plane parallel to the $\text{Pn}^*\text{-}$

bridgehead bond. The quantity of coordinated $\text{C}_4\text{H}_8\text{O}$ in solution can be measured by integration of ^1H NMR spectra with values of $x = 0.8\text{--}1.1$ typically observed. The thf resonances display no significant deviation from their expected chemical shifts, indicating that exchange of the donor ligand is fast on the NMR timescale. Three discrete hydride environments are observed of relative integration 2:2:1 (-1.09 , -2.14 , and -4.60 ppm), where the second of these resonances is well resolved as a quartet ($^2J_{\text{HH}} = 11.7$ Hz). Confident assignment of these resonances and their coupling pathways was not possible. Selective magnetization experiments were carried out in C_6D_6 with a drop of thf (vide infra), irradiating each hydride environment individually to examine any chemical exchange. No magnetization transfer was observed, indicating that the hydride ligands do not readily exchange and that the structure in solution is rather static.

The zirconium halide precursor, $\text{Pn}^*\text{Zr}_2(\mu_2\text{-Cl})_5\text{Li.thf}_x$, as observed for the titanium congener, reacts with 5 equiv of LiAlH_4 in thf over 7 days and forms a single product as judged by NMR spectroscopy. Following an analogous procedure as described for $\text{Pn}^*\text{Ti}_2(\mu_2\text{-H})_5\text{Li.thf}_x$, $[\text{Pn}^*\text{Zr}_2(\mu_2\text{-H})_4(\mu_3\text{-H})\text{Li.thf}]_2$ could be isolated in 34% yield as a pale yellow powder.

The ^1H NMR spectrum qualitatively resembles the titanium congener, with 3 $\text{Pn}^*\text{-Me}$ resonances observed indicating the presence of a time-averaged mirror plane parallel to the $\text{Pn}^*\text{-}$ bridgehead bond. The hydride resonances are somewhat shielded relative to the titanium analogue, resonating at 1.83, 1.67, and -0.36 ppm of relative integrations 2:2:1 (c.f. -1.09 , -2.14 , and -4.60 ppm for $\text{Pn}^*\text{Ti}_2(\mu_2\text{-H})_5\text{Li.thf}_x$). The implied C_{2v} symmetry indicates the formation of dimeric species in solution, as observed for $\text{Pn}^*\text{Ti}_2(\mu_2\text{-H})_5\text{Li.thf}_x$. Values for x were determined by integration of $\text{C}_4\text{H}_8\text{O}$ and $\text{Pn}^*\text{-Me}$ resonances and were found to vary between 0.5 and 0.0 ppm. Minimal deviation from the expected chemical shift of thf is observed, suggesting facile exchange of the coordinated donor on the NMR spectroscopic timescale.

Selective magnetization experiments indicate facile exchange between the two hydride environments at 1.83 and -0.36 ppm, while magnetization transfer to the third was not observed. This corresponds to exchange between H2/H3 and H4/H5 (Figure 1), while coordination of H1 remains static on the NMR timescale. This observation is slightly unexpected given the stronger metal–ligand bonds expected for zirconium relative to titanium but may result from strain associated with the radially expanded zirconium d-orbitals accommodating a hexagonal bipyramidal geometry.

The observed formation of a stable Ti(IV)-hydride is rather unusual, particularly given its synthesis from LiAlH_4 . Often

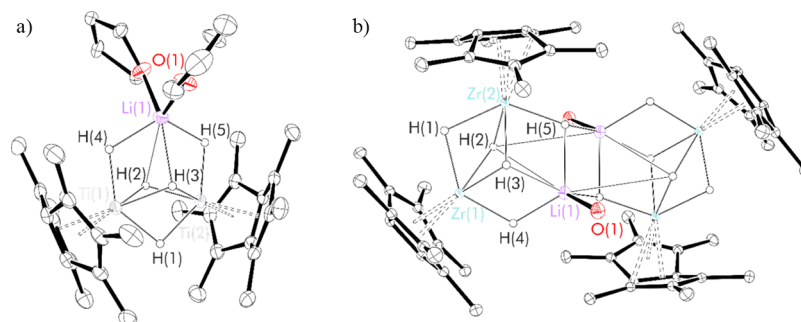


Figure 1. Thermal displacement ellipsoid plots (30% probability) of (a) $\text{Pn}^*\text{Ti}_2(\mu_2\text{-H})_5\text{Li.thf}_2$ and (b) $[\text{Pn}^*\text{Zr}_2(\mu_2\text{-H})_4(\mu_3\text{-H})\text{Li.thf}]_2$. All H atoms apart from the H1–5 have been omitted for clarity.

Table 1. Comparison of Selected Bond Lengths (Å), Angles (°), and Other Pertinent Structural Metrics

	$\text{Pn}^*\text{Ti}_2(\mu_2\text{-H})_3\text{Li.thf}_2$	$[\text{Pn}^*\text{Zr}_2(\mu_2\text{-H})_4(\mu_3\text{-H})\text{Li.thf}]_2$	$\text{Pn}^*\text{Zr}_2(\mu_2\text{-Cl})_3\text{Li.thf}_2^{33}$
fold angle	35.5(1)	32.1(8)	30.0(3)
	34.2(1)	31.2(7)	30.0(3)
M–Pn* _{cent}	1.9442(10)	2.0965(7)	2.1095 ³
M–H1 or Cl1	1.83(2)	2.01(2)	2.6431(14)
M–H2/3 or Cl2/3	1.86(3)	2.06(2)	2.6524(13)
M–H4 or Cl4	1.79(3)	1.90(2)	2.5916(12)
M–H5 or Cl5	1.86(3)	2.00(2)	2.5701(13)
H/Cl2–plane _{H1/4/5}	1.08(3)	1.28(3)	1.8103(14)
H/Cl3–plane _{H1/4/5}	1.10(3)	1.17(3)	1.8378(15)
puckering: $\sum \phi ^a$	72.80(14)	113.3(16)	143.78(4)
circumference ^b	10.88	11.9	15.16
M–M ^c	2.7874(5)	3.0816(4)	3.6549(9)

^aPuckering, given in degrees, is the sum of the magnitude of the dihedral angles around the perimeter of the metal-hydride/chloride core. For a planar structure, this value is 0°. ^bThe circumference refers to the sum of the bond lengths around the perimeter of the metal-hydride core. ^cM–M refers to the Ti–Ti or Zr–Zr distance.

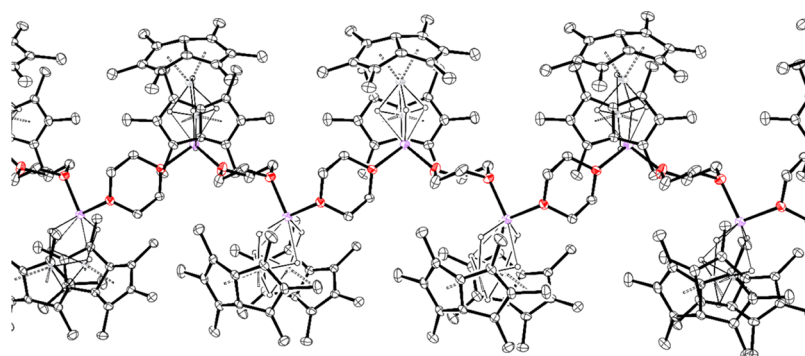


Figure 2. Thermal displacement ellipsoid plot (30% probability) of $[\text{Pn}^*\text{Ti}_2\text{H}_3\text{Li.dioxane}]_n$. All H atoms apart from H1–5 were omitted for clarity.

Ti(IV)-hydrides decompose via loss of H_2 to give reduced titanium products as is observed for Cp^*TiH_2 , which although stable as a solid decomposes in pentane solutions to form Cp^*Ti .^{12b,17} Moreover, LiAlH_4 is generally observed to form reduced titanium-hydride complexes. For example $\text{Cp}^*\text{TiH}(\text{Cl})$ reacts with LiAlH_4 to give the Ti(III) derivative, $\text{Cp}^*\text{Ti}(\mu\text{-H}_2)\text{AlH}_2\text{Et}_2\text{O}$,¹⁸ while under more forcing conditions, $(\text{Cp}^{\text{Me}4})_2\text{TiCl}_2$ reacts with LiAlH_4 to form an allyldiene complex.¹⁹ Indeed, while LiAlH_4 is certainly a viable reducing agent for $[\text{Pn}^*\text{TiCl}(\mu\text{-Cl})]_2$, it may be that this hexagonal bipyramidal motif offers a degree of kinetic stabilization with respect to H_2 loss and reduction of the metal centers; Pn^* is less sterically demanding than a corresponding bis(Cp) fragment and contributes two fewer electrons. Steric protection by intercalation of LiH and alleviation of electron deficiency by formation of 4 ($\mu\text{-H}$) bonds may favor formation of the Ti(IV)–Ti(IV) dimer over any reduced alternative.

The zirconium III/IV redox couple is less accessible than for titanium (first ionization energies: Ti = 4175 kJ/mol; Zr = 3313 kJ/mol),²⁰ which leads to the observation of less-facile reduction with LiAlH_4 . Cp^*ZrCl_2 and LiAlH_4 react to give the Zr(IV) complex, $\text{Cp}^*\text{ZrH}(\mu\text{-H})_2\text{AlH}_2$, which can be further reacted with $n\text{BuLi}$ to form the anionic zirconocene hydride, $[\text{Cp}^*\text{ZrH}_3]^-$.²¹ As expected, the three hydride ligands in these complexes are arranged in a coplanar fashion, due to the projection of CpR_2Zr frontier orbitals in a single plane, in contrast to those observed for $[\text{Pn}^*\text{Zr}_2(\mu_2\text{-H})_4(\mu_3\text{-H})\text{Li.thf}]_2$. While the Cp analogue is less stable,²² its synthesis from

Cp_2ZrCl_2 and LiAlH_4 can be realized by inclusion of an amine donor to stabilize the complex, forming $\text{Cp}_2\text{ZrH}(\mu\text{-H})_2\text{AlH}_2(\text{NR}_3)$ (NR_3 = quinuclidine, 1-azabicyclo[2.2.2]octane; NMe_3).²³

Reduced species can be accessed from Cp_2ZrCl_2 by addition of substoichiometric amounts of CoBr_2 alongside LiAlH_4 , which allows for the formation of $[(\text{Cp}_2\text{Zr})(\mu\text{-H})(\mu\text{-H})_2\text{AlCl}_2]$, in which the Zr–H–Al core displays a hexagonal planar geometry similar to that reported for the Pn^* complexes.²⁴ Hydrogenation of the doubly silylene-bridged *ansa*-zirconocene, $[\{(\text{Me}_2\text{Si})_2(\eta^5\text{-C}_5\text{H}_3)_2\}\text{ZrMe}_2]$, forms the structurally characterized trimetallic hydride cluster, $[\{(\text{Me}_2\text{Si})_2(\eta^5\text{-C}_5\text{H}_3)_2\}\text{Zr}]_3(\mu_3\text{-H})_2(\mu_2\text{-H})_3$,²⁵ although use of the hydride transfer reagent, NaBEt_3H , produces the more commonly observed zirconium-hydride motif, $[\{(\text{Me}_2\text{Si})_2(\eta^5\text{-C}_5\text{H}_3)_2\}\text{ZrH}]_2(\mu_2\text{-H})_2$.²⁶

Structure and Bonding of Group 4 Lithium Metal Hydride Clusters: $\text{Pn}^*\text{M}_2(\mu_2\text{-H})_3\text{Li.thf}_x$. Single crystals of both $\text{Pn}^*\text{Ti}_2(\mu_2\text{-H})_3\text{Li.thf}_2$ and $[\text{Pn}^*\text{Zr}_2(\mu_2\text{-H})_4(\mu_3\text{-H})\text{Li.thf}]_2$ suitable for X-ray diffraction were grown by slow evaporation of thf solutions at room temperature (Figure 1 and Table 1).

The structure is analogous to that of the zirconium(IV) complex, $\text{Pn}^*\text{Zr}_2(\mu_2\text{-Cl})_3\text{Li.thf}_x$, and can be similarly rationalized in terms of its Lewis structure as two Ti(IV) centers with intercalated LiH. The central metal-hydride core forms a distorted hexagonal bipyramid, which appears to be a favored structural motif of group 4 Pn^* complexes. The exposed lithium ion at the cluster's apex is weakly bound to the donor

solvent, and the complex was also serendipitously crystallized as a mixed thf-benzene solvate. Alternatively, 1,4-dioxane was found to coordinate more strongly, producing similar spectroscopic features to the bis(thf) solvate. Single crystals of the dioxane complex were obtained from slow evaporation of a benzene solution (Figure 2).

The bidentate donor bridges across two neighboring lithium ions, forming a 1D polymer composed of metal-hydride clusters and dioxane linker units. Beyond the polymeric nature of this material, the key bond lengths and angles are similar to those of the bis(thf) complex (see the Supporting Information).

The observation of hexagonal bipyramidal geometry contrasts with the preference of early transition metal Cp_2M fragments to adopt the more familiar bent metallocene structure found for Cp_2ZrCl_2 .²⁷ Indeed Cp_2M fragments with vacant coordination sites display a preference for planar coligand bonding, as is observed for Cp_2TaH_3 ,^{28,29} rather than the fourfold coligand coordination that permits formation of this trimetallic bipyramid.

Density functional theory (DFT) calculations were carried out on $Pn^*_2Ti_2(\mu_2-H)_5Li.THF_2$ at the B3LYP level of theory,³⁰ with Ahlrichs' triple- ζ basis set employed for heavy elements and hydride ligands.³¹ Geometry optimizations reproduced the experimental data well, although some variation was observed in the orientation of coordinated thf. In the following discussion, the molecular symmetry is approximated as C_{2v} , which is valid in the absence of coordinated THF and assumes that this coordinated solvent has negligible effect on the frontier molecular orbitals. The hexagonal plane is primarily supported by two orbitals of the Pn^*Ti fragment: one of a_1 symmetry with $d_{x^2-y^2}$ and d_{z^2} character, projecting electron density above and below the plane bisecting the Pn^* -bridgehead bond, bonding to the whole hydride system, and a second of b_1 symmetry, predominantly d_{yz} in character. Unlike analogous Cp_2Ti fragments, an orthogonal b_1 symmetric orbital is also accessible, which supports $Ti-H_2/H_3$ bonding, securing the hydride caps of the hexagonal bipyramid (Figure 3).

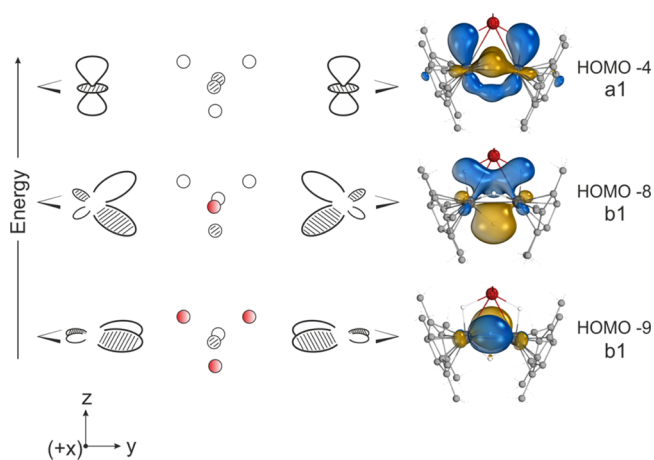


Figure 3. Primary Ti–H bonding orbitals calculated for $Pn^*_2Ti_2(\mu_2-H)_5Li.thf_2$, illustrating the projection of electron density in two orthogonal planes: zy (HOMO-4 and HOMO-8) and xy (HOMO-9). Red circles represent hydrogen atoms uninvolved in bonding for each MO.

This geometry, rarely encountered for Cp_2Ti , is therefore a consequence of electron density projected in two orthogonal planes. Interestingly, the calculations also predict a metal–metal bonding interaction between the titanium centers, with a calculated Mayer bond order of 0.616.³² Indeed, the distance between the two titanium ions of 2.79 Å (2.82 Å calculated) is well below the sum of the van der Waals radii (4.30 Å for titanium). No molecular orbitals were found to uniquely describe a metal–metal bonding interaction, with this orbital overlap clearly mediated by bridging hydride ligands.

The solid-state structure of $[Pn^*_2Zr_2(\mu_2-H)_4(\mu_3-H)Li.thf]_2$ is C_1 symmetric, bridging through two apical Li–H fragments, each stabilized by a single thf molecule. The basic structure of the metal-hydride core consists of edge-fused distorted hexagonal bipyramids, similar to those found in $Pn^*_2Ti_2(\mu_2-H)_5Li.thf_2$, albeit with more extensive puckering observed, which may be a consequence of dimerization. A comparison of key bond lengths and angles is provided in Table 1 for $Pn^*_2Ti_2(\mu_2-H)_4(\mu_3-H)Li.thf_2$ and $[Pn^*_2Zr_2(\mu_2-H)_4(\mu_3-H)Li.thf]_2$, along with $Pn^*_2Zr_2(\mu_2-Cl)_5Li.thf_2$, which also displays this hexagonal bipyramid motif.

Contraction of ionic radii from zirconium to titanium leads to a large increase in the fold angle measured for $Pn^*_2Ti_2(\mu_2-H)_5Li.thf_2$, along with a decrease in $M-Pn^*_{cent}$ and $M-H$ bond lengths. This leads to compression of the hexagonal bipyramid, which can be straightforwardly visualized by considering both the decreased circumference of the metal-hydride core and the decreased $H_2/3-Plane_{H1/4/5}$ bond lengths corresponding to narrowing of the pyramidal apices. As would be expected based on a qualitative examination of the structure, more extensive puckering is observed for $[Pn^*_2Zr_2(\mu_2-H)_4(\mu_3-H)Li.thf]_2$, although given the further increase observed for $Pn^*_2Zr_2(\mu_2-Cl)_5Li.thf_2$, this is probably not simply a consequence of the former's greater nuclearity.

DFT calculations were carried at the B3LYP level theory using the same basis set as for $Pn^*_2Ti_2(\mu_2-H)_5Li.thf_2$, which reproduced the experimental data adequately. Similar metal–metal bonding interactions are predicted with $Zr-Zr$ bond orders of 0.463 and 0.468, lower than those computed for the titanium analogue. This mirrors an increase in the intermetallic distance to 3.12 Å (3.08 Å observed experimentally vs 2.79 Å for $Pn^*_2Ti_2(\mu_2-H)_5Li.thf_2$), which remains well below the sum of the van der Waals radii for zirconium, 4.60 Å. As before no molecular orbital was calculated to uniquely describe this bonding interaction, with the lower symmetry resulting from dimerization leading to greater orbital mixing.

Reactivity of Group 4 Lithium Metal Hydride Clusters: $Pn^*_2M_2(\mu_2-H)_5Li.thf_x$. $Pn^*_2Ti_2(\mu_2-H)_5Li.thf_2$ is surprisingly inert toward many small molecules. When exposed to stoichiometric or excess 2-butyne in C_6D_6/THF , no reaction was observed up to 60 °C by 1H NMR spectroscopy. Similarly, the complex was found to be inert toward alkenes: *cis*-1,2-diphenylethylene, cyclohexene, and ethylene did not react. Under 1 bar D_2 , trace amounts of HD can be observed by 1H NMR spectroscopy (4.51 ppm, t, $^1J_{H-D} = 43$ Hz), characteristic of exchange. However, after heating to 60 °C for 4 days, the extent of deuterium incorporation was still insufficient to be resolved by 2H NMR spectroscopy. The sluggish reactivity of $Pn^*_2Ti_2(\mu_2-H)_5Li.thf_x$ may be a result of the crowded coordination environment around the titanium centers preventing approach of these small molecules.

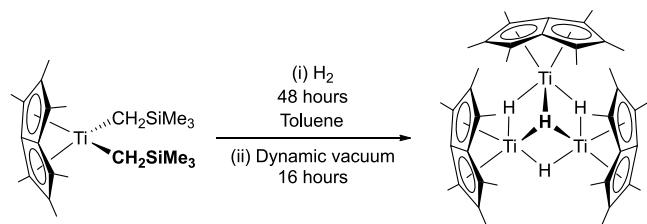
Although the deuterium complex could not be formed by H–D exchange, its synthesis was achieved by the reaction of

LiAlD₄ in thf over 4–7 days. Following extraction into benzene and subsequent crystallization from thf, Pn*₂Ti₂(μ₂-D)₅Li.thf_x was obtained as a crystalline yellow solid in 64% yield. The ¹H NMR spectrum displays the same Pn*–Me resonances unshifted relative to the hydride analogue, with no peaks corresponding to the complex observed below 2.02 ppm. *x* was found to be 0.96 by integration against Pn*–Me resonances, with no significant deviation in the THF chemical shift observed. The deuteride resonances were observed by ²H NMR spectroscopy at –1.06, –2.12, and –4.49 ppm (c.f. –1.09, –2.14, and –4.60 ppm for the corresponding hydride resonances), demonstrating the successful synthesis of the isotopically labeled complex. Comparison of FTIR spectra of Pn*₂Ti₂(μ₂-H)₅Li.thf_x and Pn*₂Ti₂(μ₂-D)₅Li.thf_x allows for the definitive assignment of Ti–H/D stretching frequencies. An intense peak at 1507 cm^{–1} is observed for the hydride complex, which is shifted to 1099 cm^{–1} on perdeuteration, which is in good agreement with the value calculated using the reduced mass formula (1077 cm^{–1}). A second hydride-stretch observed at 1291 cm^{–1} is red-shifted to 941 cm^{–1}, in close agreement with a predicted value of 922 cm^{–1}.

In contrast, for [Pn*₂Zr₂(μ₂-D)₄(μ₃-D)Li.thf_x]₂, there is facile D₂ incorporation, with complete disappearance of hydride resonances observed after 4 days under 1 bar D₂ at room temperature. This is accompanied by HD formation, which can be clearly resolved by ¹H NMR spectroscopy. The deuteride complex was synthesized on a preparative scale by the reaction of Pn*₂Zr₂Cl₃Li.THF_x and LiAlD₄ in thf. Extraction into benzene and crystallization from thf allowed for the isolation of [Pn*₂Zr₂(μ₂-D)₄(μ₃-D)Li.thf_x]₂ in 41% yield as a yellow powder.

A Group 4 Trimetallic Hydride Cluster: Pn*₃Ti₃(μ₂-H)₃(μ₃-H). The purple titanium alkyl precursor, Pn*Ti(CH₂SiMe₃)₂, was first synthesized by the salt elimination reaction of [Pn*TiCl](μ–Cl)₂ with 2 equiv of NaCH₂SiMe₃. On exposing a C₆D₆ solution of Pn*Ti(CH₂SiMe₃)₂ to H₂, the solution turned black-green over the course of 48 h. ¹H NMR spectra indicated the consumption of the starting material and the formation of new diamagnetic and paramagnetic species alongside SiMe₄ (Scheme 2). Only after drying the sample

Scheme 2. Synthesis of Pn*₃Ti₃(μ₂-H)₃(μ₃-H)



under dynamic vacuum was a clean, diamagnetic complex obtained, with 2 Pn*–Me resonances resolved at 2.31 and 2.16 ppm in the ¹H NMR spectrum, alongside a single hydride resonance at –2.91 ppm integrated to 4H. Single crystals suitable for an X-ray diffraction study were grown from slow evaporation of a benzene solution with 1 drop of added toluene, which confirms the formation of the trimetallic hydride cluster Pn*₃Ti₃(μ₂-H)₃(μ₃-H) (Figure 4 and Table 2).

Structure and Bonding of a Group 4 Trimetallic Hydride Cluster: Pn*₃Ti₃(μ₂-H)₃(μ₃-H). The central metal-hydride core adopts a hexagonal pyramidal geometry with one face uncapped, similar to the complexes discussed previously.

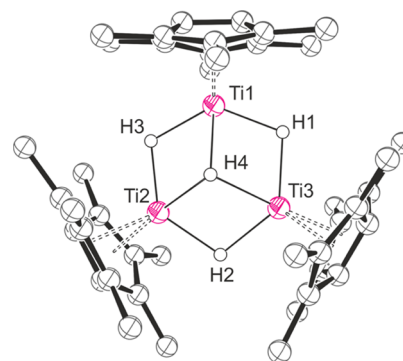


Figure 4. Thermal displacement ellipsoid plot (30% probability) of Pn*₃Ti₃(μ₂-H)₃(μ₃-H). All H atoms apart from H1–4 are omitted for clarity. H4 is shown in one of the two partially occupied positions.

Table 2. Comparison of Selected Bond Lengths (Å), Angles (°), and Other Pertinent Structural Metrics of Pn*₃Ti₃(μ₂-H)₃(μ₃-H) with [{(Me₂Si)₂(η⁵-C₅H₃)₂}Zr]₃H₅

	Pn* ₃ Ti ₃ (μ ₂ -H) ₃ (μ ₃ -H)	[{(Me ₂ Si) ₂ (η ⁵ -C ₅ H ₃) ₂ }Zr] ₃ H ₅ ²⁵
fold angle	33.43(10) 32.27(9) 32.27(9)	-
M–Pn* _{cent} / C _{Pcent}	1.9810(10)	2.2648(10)
M–H1	1.78(3)	1.963(19)
M–H2	1.84(3)	2.16(2)
M–H3	1.84(3)	1.94(2)
M–H4	1.995(16)	1.94(2)
M–H5		2.16(2)
H4–plane _{H1/3/4}	1.17(2)	0.93(2)
H5–plane _{H1/3/4}		0.93(2)
puckering: Σ φ ^a	82(6)	28.4(11)
circumference ^b	10.91(24)	11.67(12)
M–M ^c	2.9454(9)	3.2939(10)

^aPuckering, given in degrees, is the sum of the magnitude of the dihedral angles around the perimeter of the metal-hydride core. For a planar structure, this value is 0°. ^bThe circumference refers to the sum of the bond lengths around the perimeter of the metal-hydride core. ^cM–M given as an average of three values.

The hydride atoms were crystallographically located, although H4 was found to be partially disordered across both faces of the hexagon. A comparison of key bond lengths and angles is provided in Table 2 alongside [{(Me₂Si)₂(η⁵-C₅H₃)₂}Zr]₃H₅,²⁵ which is the closest structural analogue found in the literature.

The fold angles are shallower for Pn*₃Ti₃(μ₂-H)₃(μ₃-H) than for Pn*₂Ti₂(μ₂-H)₅Li.thf₂, which is likely a result of formal reduction of two titanium centers to Ti(III). Elongation of the apical hydride–titanium bond is observed, which is also mirrored in [{(Me₂Si)₂(η⁵-C₅H₃)₂}Zr]₃H₅. Slightly surprising is the contraction of bipyramid apices for [{(Me₂Si)₂(η⁵-C₅H₃)₂}Zr]₃H₅ relative to Pn*₃Ti₃(μ₂-H)₃(μ₃-H), despite an increased ionic radius in the former case. The titanium complex is more puckered than the zirconium analogue, which may be facilitated by the symmetrical displacement of capping hydride ligands in [{(Me₂Si)₂(η⁵-C₅H₃)₂}Zr]₃H₅. Similarly, Pn*₂Ti₂(μ₂-H)₅Li.thf₂, with two capping hydride ligands, displays a less-puckered structure than Pn*₃Ti₃(μ₂-H)₃(μ₃-H), suggesting that the structural stabilization afforded by this symmetrical ligand placement outweighs any distorting effects

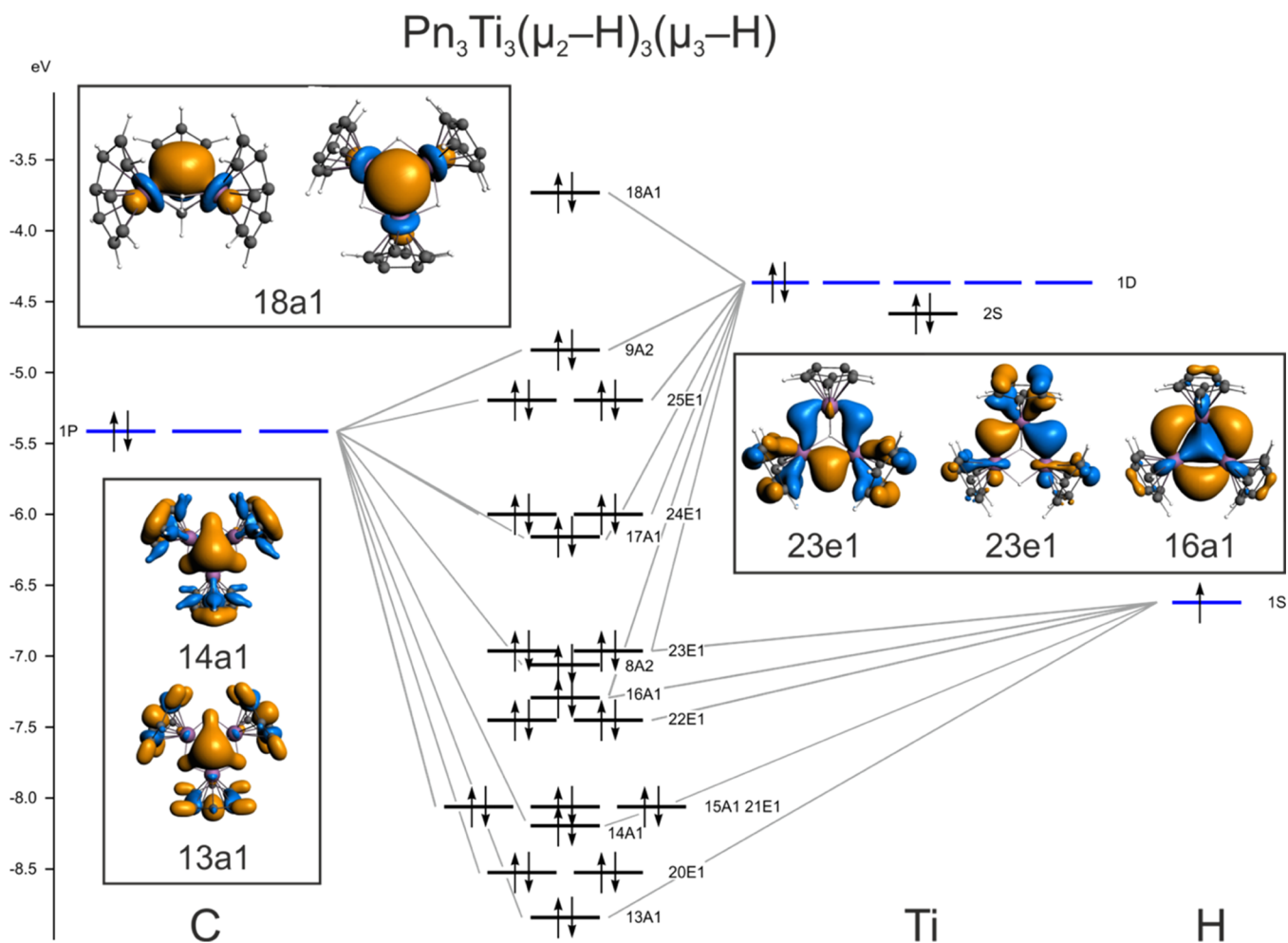


Figure 5. Fragment molecular orbital diagram for $\text{Ti}_3\text{Pn}^*_3(\mu_2\text{-H})_3(\mu_3\text{-H})$, with key Ti–Ti and Ti–H bonding interactions highlighted.

resulting from hetero-metal incorporation. Despite this, the circumference of $\text{Pn}^*_3\text{Ti}_3(\mu_2\text{-H})_3(\mu_3\text{-H})$ is almost identical to that found for $\text{Pn}^*_2\text{Ti}_2(\mu_2\text{-H})_5\text{Li.tfhf}_2$, although a slight increase in average Ti–Ti distance is observed.

$\text{Pn}^*_3\text{Ti}_3(\mu_2\text{-H})_3(\mu_3\text{-H})$ is a mixed-valence hydride cluster with d-electron count $d^0\text{-}d^1\text{-}d^1$, which might be expected to behave as a paramagnet. However, spectroscopic evidence indicates that it is diamagnetic. DFT calculations were therefore carried out to probe the origin of this diamagnetism, gain insight into the nature of bonding in the complex, and investigate energetically accessible derivatives that may aid in the rationalization of the electron paramagnetic resonance (EPR) data.

Density functional calculations were carried out using the Amsterdam density functional package³⁴ and triple- ζ quality basis sets augmented with a one polarization function (ADF basis TZP). The local density approximation of Vosko, Wilk, and Nusair³⁵ was used together with the exchange correlation corrections of Becke and Perdew (BP86).³⁶ The geometries of both $\text{Ti}_3\text{Pn}_3(\mu_2\text{-H})_3(\mu_3\text{-H})$ and $\text{Ti}_3\text{Pn}^*_3(\mu_2\text{-H})_3(\mu_3\text{-H})$ were successfully optimized with C_{3v} symmetry found for the Pn complex and the Ti_3H_4 core of the Pn^* analogue. For simplicity, a bonding analysis was carried out on $\text{Ti}_3\text{Pn}_3(\mu_2\text{-H})_3(\mu_3\text{-H})$ (Figure 5).

The HOMO, 18a1, is a cluster-based bonding orbital composed primarily of metal d₂ orbitals, projecting onto the vacant face of the hexagonal pyramid. The diamagnetism of the

complex can be understood to result from the overlap of these d₂ orbitals, which accommodates the two otherwise unpaired electrons. The next six lower energy orbitals describe titanium–pentalene bonding interactions, which are followed by a set of orbitals, some of which have Ti–H bonding characteristics (23e1 and 16a1) that describe the Ti–H–Ti 3c–2e bonds in a localized bonding model. The apical hydride bonding interaction is primarily exhibited lower in the manifold in orbitals 14a1 and 13a1, with the edge-bridging hydrides contributing to lesser extent.

Calculations were also performed on $\text{Ti}_3\text{Pn}^*_3(\mu_2\text{-H})_3(\mu_3\text{-H})_2$, paramagnetic species, and $\text{Ti}_3\text{Pn}_3(\mu_2\text{-H})_3(\mu_3\text{-H})_2$. Various starting structures were attempted, the lowest energy of which was a D_{3h} symmetric structure with the additional hydride atom localized on the exposed face of the hexagonal pyramid. The extra electron occupies a SOMO, 26e1, localized on the three titanium atoms (Pn analogue shown in Figure 6). Jahn–Teller distortion from pure D_{3h} symmetry is therefore predicted, but given the weak bonding/antibonding characteristics of the 26e1 orbital, such a distortion might not be static. As discussed in relation to $\text{Pn}^*_2\text{Ti}_2(\mu_2\text{-H})_5\text{Li.tfhf}_2$, this hexagonal bipyramidal metal–hydride core can be understood to result from the orthogonal disposition of the PnTi frontier molecular orbitals. The most closely related complex previously reported is the trimetallic zirconium hydride cluster $[\{(\text{Me}_2\text{Si})_2(\eta^5\text{-C}_5\text{H}_3)_2\}\text{Zr}]_3(\mu_3\text{-H})_2(\mu_2\text{-H})_3$, formally Zr(IV)/Zr(IV)/Zr(III), which was identified in the solid-state and also

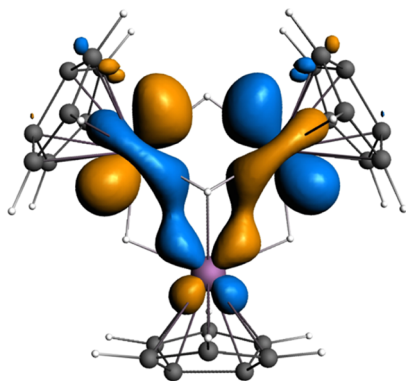


Figure 6. SOMO calculated for the paramagnetic hydride complex, $\text{Ti}_3\text{Pn}_3(\mu_2\text{-H})_3(\mu_3\text{-H})_2$.

contains the same structural motif as for $\text{Ti}_3\text{Pn}^*_3(\mu_2\text{-H})_3(\mu_3\text{-H})_2$.²⁵

Reactivity of a Group 4 Trimetallic Hydride Cluster: $\text{Pn}^*_3\text{Ti}_3(\mu_2\text{-H})_3(\mu_3\text{-H})$. A solution of $\text{Pn}^*_3\text{Ti}_3(\mu_2\text{-H})_3(\mu_3\text{-H})$ in C_7D_8 was exposed to 1 bar D_2 at 298 K and analyzed by NMR spectroscopy after 15 minutes. The ^1H NMR spectrum indicated the presence of paramagnetic products even after this short reaction time, with broad overlapping resonances observed between 5 and 1 ppm, alongside the starting material and other unidentified diamagnetic resonances. ^2H NMR spectra displayed a new resonance at -3.1 ppm, resulting from deuterium exchange, although no resonance corresponding to HD could be observed. After 48 h, the ^1H NMR spectrum was somewhat similar to that observed under H_2 . However, clear differences can be observed both in the number and position of the paramagnetic and diamagnetic components (Supporting Information).

The rapid reaction with D_2 contrasts dramatically with the slow exchange observed for $\text{Pn}^*_2\text{Ti}_2(\mu_2\text{-H})_3\text{Li.tthf}_w$, which is presumably a consequence of the vacant coordination site presented by $\text{Pn}^*_3\text{Ti}_3(\mu_2\text{-H})_3(\mu_3\text{-H})$. After exposing the paramagnetic mixture to dynamic vacuum and redissolving in C_7D_8 , the diamagnetic deuterated complex, $\text{Pn}^*_3\text{Ti}_3(\mu_2\text{-D})_3(\mu_3\text{-D})$, could be observed by NMR spectroscopy. Two $\text{Pn}^*\text{-Me}$ resonances at 2.30 and 2.15 ppm are the only ones observed by ^1H NMR spectroscopy, with a corresponding deuteride resonance at -3.1 ppm. $\text{Pn}^*_3\text{Ti}_3(\mu_2\text{-D})_3(\mu_3\text{-D})$ was synthesized on a preparative scale by an analogous method to $\text{Pn}^*_3\text{Ti}_3(\mu_2\text{-H})_3(\mu_3\text{-H})$, with D_2 gas instead of H_2 . The product was obtained in 65% yield as a black crystalline solid.

FTIR spectroscopy of the hydride and deuteride complexes displays stretches at 1310 and 936 cm^{-1} , respectively, which is in close agreement with values predicted by the reduced mass formula (1310 and 944 cm^{-1}). A new peak at 1043 cm^{-1} in the spectrum of $\text{Pn}^*\text{Ti}_3\text{D}_4$ could not be related by its reduced mass to a corresponding peak in the spectrum of $\text{Pn}^*_3\text{Ti}_3(\mu_2\text{-H})_3(\mu_3\text{-H})$ (expected value 1457 cm^{-1}) due to overlap with an intense broad peak at 1444 cm^{-1} assigned to $\text{Pn}^*\text{C}=\text{C}$ bond stretching.

Given the observation of paramagnetism under H_2/D_2 , $\text{Pn}^*_3\text{Ti}_3(\mu_2\text{-H})_3(\mu_3\text{-H})$ was studied by X-band EPR spectroscopy in the presence of these gases. A toluene solution of $\text{Pn}^*_3\text{Ti}_3(\mu_2\text{-H})_3(\mu_3\text{-H})$ was pressurized with 1 bar H_2 in a J-Youngs Quartz EPR tube, and spectra were collected after 30 min, 6 h, and 48 h.

Complicated speciation was inferred from the observation of a number of paramagnetic components between $g = 1.96$ and 1.98. Due to the overlap and weak intensity of these resonances, it is not possible to confidently assign the number of minor components. The major component at $g = 1.993$ is clearly resolved 30 minutes after gas addition and is observed to increase in relative intensity over the course of 48 h, with intermediate conversion observed at 6 h. That the additional components are the result of speciation and not decomposition was confirmed by repeating the reaction at a fivefold increase in concentration (25 mM vs 5 mM), which produced these minor components to the same extent. Indeed, the presence of both paramagnetic and diamagnetic components by ^1H NMR spectroscopy under H_2 pressure further alludes to the formation of multiple products and it could be envisaged that variation in nuclearity and hydride/deuteride content under H_2/D_2 may lead to the observed speciation. Unfortunately, no hyperfine coupling to the hydride ligands was observed, which limits additional insight into the nature of these complexes.

Repeating the reaction with D_2 , similar reactivity was observed. The same resonance at $g = 1.993$ is observed, formed within 30 minutes and increasing in intensity over the course of 48 h. However, the distribution of minor components is altered relative to H_2 , with a more intense resonance at $g = 1.972$ resolved under D_2 after 48 h. No additional splitting of peaks is observed ($D, S = 1; H, S = 1/2$), confirming the absence of hyperfine coupling at the experimental resolution.

Attempts to crystallize the major product from saturated toluene solutions of $\text{Pn}^*_3\text{Ti}_3(\mu_2\text{-H})_3(\mu_3\text{-H})$ under H_2 pressure were unsuccessful, preventing the conclusive identification of these paramagnetic complexes in the solid state. Some plausible structures for this major paramagnetic component could therefore be proposed. $\text{Pn}^*_3\text{Ti}_3(\mu_2\text{-H})_3(\mu_3\text{-H})_2$, related to the diamagnetic starting complex by incorporation of an additional hydride ligand across the open face of the hexagonal bipyramid. Alternatively, it could be envisaged that variation in the nuclearity of the metal-hydride product could occur, forming complexes such as the mixed valence hydride dimer, $(\text{Pn}^*\text{Ti})_2(\mu\text{-H})_3$, displaying a Ti/H ratio of 1:1.5 (1:1.33 for the diamagnetic starting complex).

An interesting comparison can be drawn between $\text{Pn}^*_3\text{Ti}_3(\mu_2\text{-H})_3(\mu_3\text{-H})$ and the titanium half-sandwich hydride, $[(\text{Cp}'\text{Ti})_3(\mu_3\text{-H})(\mu_2\text{-H})_6]$ ($\text{Cp}' = \text{C}_2\text{Me}_4\text{SiMe}_3$), formed by hydrogenation of $\text{Cp}'\text{Ti}(\text{CH}_2\text{SiMe}_3)_3$.^{10c} The structure can be considered analogous to that of $\text{Pn}^*_3\text{Ti}_3(\mu_2\text{-H})_3(\mu_3\text{-H})$, only with six hydride ligands bracing the hexagonal plane to account for the substitution of Pn^* for a monoanionic carbocycle, Cp' . This contrasts with the tetrametallic clusters observed following hydrogenation of $\text{Cp}'\text{M}(\text{CH}_2\text{SiMe}_3)_3$ ($\text{M} = \text{Zr}, \text{Hf}$), where all four metal centers are in the +3 oxidation state.^{10d}

$[(\text{Cp}'\text{Ti})_3(\mu_3\text{-H})(\mu_2\text{-H})_6]$ displays remarkable reactivity, cleaving the dinitrogen triple bond to form two bridging $[\text{NH}]^{2-}$ ligands in 90% yield,^{10c} as well as activating benzene to form methylcyclopentenyl derivatives.^{10a,b} Unfortunately, despite their structural similarity, comparable transformations were not observed with in $\text{Pn}^*_3\text{Ti}_3(\mu_2\text{-H})_3(\mu_3\text{-H})$. The complex is stable in benzene and does not react with N_2 (up to 4 bar). With CO, decomposition is observed, similar to the reported reactivity with $\text{Pn}^*_2\text{Ti}_2(\mu_2\text{-H})_3\text{Li.tthf}_w$, while with CO_2 no evidence for hydride transfer is observed although a number

of new hydride resonances could be resolved by NMR spectroscopy, perhaps resulting from the formation of titanium–oxide–hydride derivatives. The complex is unreactive toward 2-butyne, although reactivity is observed with ethylene. Following the reaction by ^1H NMR spectroscopy, slow consumption of the starting material was observed alongside the formation of a large number of Pn^*-Me and the appearance of eight new hydride environments in the region -0.49 to -6.54 ppm. This divergent reactivity of complexes that appear electronically and structurally so related highlights the importance of the ancillary ligand set in directing the chemistry of metal hydrides. Although clean reaction with small molecules could not be realized, it is interesting to contrast the reactivity of $\text{Pn}^*_3\text{Ti}_3(\mu_2\text{-H})_3(\mu_3\text{-H})$ to the stability of $\text{Pn}^*_2\text{Ti}_2(\mu_2\text{-H})_5\text{Li.thf}_x$ under similar conditions, which may be driven by the presence of a suitable vacancy in the coordination sphere of the metal centers in $\text{Pn}^*_3\text{Ti}_3(\mu_2\text{-H})_3(\mu_3\text{-H})$.

CONCLUSIONS

The preparation of new permethylpentalene, Pn^* , metal-hydride complexes has been described, $\text{Pn}^*_2\text{Ti}_2(\mu_2\text{-H})_5\text{Li.thf}_x$ and $[\text{Pn}^*_2\text{Zr}_2(\mu_2\text{-H})_5\text{Li.thf}_x]_2$, which can both be accessed from the corresponding M(IV) chloride precursor and LiAlH_4 in thf. A number of intermediate hydride species were observed spectroscopically. The titanium-hydride complex is not fluxional on the NMR spectroscopic timescale and does not readily exchange with D_2 , while the zirconium congener undergoes chemical exchange between two of the three observed hydride environments. As expected, given its fluxional solution-phase behavior, the zirconium complex also readily exchanged with D_2 gas in a $\text{C}_6\text{D}_6/\text{thf}$ solution. The deuteride complexes, $\text{Pn}^*_2\text{Ti}_2(\mu_2\text{-D})_5\text{Li.thf}_x$ and $[\text{Pn}^*_2\text{Zr}_2(\mu_2\text{-D})_5\text{Li.thf}_x]_2$, were successfully synthesized using LiAlD_4 and characterized by NMR and FTIR spectroscopy. Both complexes were structurally characterized with a variety of solvents coordinated to the apical lithium atom and demonstrate an unusual hexagonal bipyramidal geometry. In the case of $[\text{Pn}^*_2\text{Zr}_2(\mu_2\text{-H})_4(\mu_3\text{-H})\text{Li.thf}]_2$, edge-fused bipyramids are observed in the solid state, forming a more puckered hydride cluster. This geometry has only rarely been encountered previously and can be rationalized by DFT calculations as the resulting frontier orbital electron density projected in two orthogonal planes, in contrast with the coplanar orientation found for Cp_2M complexes.

The diamagnetic mixed-valence titanium hydride cluster, in $\text{Pn}^*_3\text{Ti}_3(\mu_2\text{-H})_3(\mu_3\text{-H})$, was also investigated. Surprisingly, under H_2 , the complex reversibly forms a large number of unidentified paramagnetic components, which are all converted to $\text{Pn}^*_3\text{Ti}_3(\mu_2\text{-H})_3(\mu_3\text{-H})$ under dynamic vacuum overnight. The proposed structure was crystallographically confirmed and further corroborated by DFT calculations, which illustrated the formation of a metal-cluster bonding orbital responsible for the diamagnetism of the complex. These new hydride complexes provide interesting comparisons, both in terms of solid-state structures and reactivity, to related cyclopentadienyl analogues.

EXPERIMENTAL DETAILS

All manipulations were carried out using standard Schlenk line or drybox techniques under an atmosphere of dinitrogen or argon. Protio solvents were degassed by sparging with dinitrogen, dried by passing through a column of activated sieves (pentane, hexane, toluene, and

benzene) and stored over potassium mirrors, or distilled from sodium metal (thf) and stored over activated 4 Å molecular sieves, or distilled from sodium-potassium alloy (diethyl ether) and stored over a potassium mirror. Deuterated solvents were dried over potassium (C_6D_6 , C_7D_8) or CaH_2 ($\text{C}_4\text{D}_8\text{O}$), distilled under reduced pressure, and freeze–pump–thaw degassed three times prior to use.

^1H NMR spectra were recorded at 298 K, unless otherwise stated, on Bruker AVIII 400 nanobay or Bruker AVIII 500 spectrometers, and $^{13}\text{C}\{^1\text{H}\}$ or ^{13}C NMR spectra, on the same spectrometers at operating frequencies of 100 and 125 MHz, respectively. Two-dimensional $^1\text{H}-^1\text{H}$ and $^{13}\text{C}-^1\text{H}$ correlation experiments were used, when necessary, to confirm ^1H and ^{13}C NMR assignments. All NMR spectra were referenced internally to residual protio solvent (^1H) or solvent (^{13}C) resonances and are reported relative to tetramethylsilane ($\delta = 0$ ppm). Chemical shifts are quoted in δ (ppm), and coupling constants, in Hertz. Elemental analyzes were carried out at London Metropolitan University. FTIR spectra were prepared in a glove box as pressed KBr discs. Spectra were recorded on a Nicolet iSS Thermo Scientific spectrometer. $\text{Pn}^*_3\text{Ti}_3(\mu_2\text{-H})_3(\mu_3\text{-H})$ was studied by X-band EPR spectroscopy in the presence of H_2 or D_2 . A toluene solution of $\text{Pn}^*_3\text{Ti}_3(\mu_2\text{-H})_3(\mu_3\text{-H})$ was pressurized with 1 bar H_2 in a J-Young Quartz EPR tube, and spectra were collected after 30 minutes, 6 h, and 48 h.

The following compounds were synthesized according to a literature procedure: $[\text{Pn}^*\text{TiCl}(\mu\text{-Cl})]_2$ and $[\text{ZrPn}^*(\mu\text{-Cl})_{3/2}]_2(\mu\text{-Cl})_2\text{Li.thf}_x$.³³

$\text{Pn}^*_2\text{Ti}_2(\mu_2\text{-H})_5\text{Li.thf}_x$. $[\text{Pn}^*\text{TiCl}(\mu\text{-Cl})_2$ (0.250 g, 0.410 mmol) and LiAlH_4 (0.777 g, 2.05 mmol) were dissolved in thf (10 mL) and stirred at room temperature for 4 days. An aliquot was taken, and if necessary, further LiAlH_4 was added and stirred for 36 h. Once completed, the volatiles were removed under vacuum and the gray solid was extracted with benzene (4×7 mL) and filtered through celite. The combined extracts were concentrated to ca. 10 mL, and the mixture was lyophilized under dynamic vacuum to give a flocculant brown solid. This was dissolved in a minimum volume of thf (3×3 mL) and filtered a second time through celite. This solution was concentrated to ca. 2–3 mL and cooled to -80 °C for 1 week, depositing bright yellow crystals of $\text{Pn}^*_2\text{Ti}_2(\mu_2\text{-H})_5\text{Li.thf}_2$, which were isolated by filtration and washed once with -78 °C pentane (1×3 mL). The solid was dried under dynamic vacuum for 4 h, allowing for the isolation of $\text{Pn}^*_2\text{Ti}_2(\mu_2\text{-H})_5\text{Li.thf}_x$ in 57% yield (0.127 g, 0.234 mmol, $x = 0.9$, determined by ^1H NMR spectroscopy). Single crystals of $\text{Pn}^*_2\text{Ti}_2(\mu_2\text{-H})_5\text{Li.thf}_2$ suitable for an X-ray diffraction study were grown by slow evaporation of a thf solution. ^1H NMR (400 MHz, 298 K, $\text{C}_4\text{D}_8\text{O}$) δ (ppm): 2.34 (s, 6H, 1,7-Me-Pn*), 2.28 (s, 6H, 3,5-Me-Pn*), 1.96 (s, 6H, 2,6-Me-Pn*), -1.09 (br s, $\nu_{1/2} = 29$ Hz, 2H, Ti-H), -2.14 (q, 2H, $^2J_{\text{H-H}} = 11.7$ Hz, Ti-H), -4.60 (m, 1H, Ti-H). ^1H NMR (400 MHz, 298 K, $\text{C}_6\text{D}_6/\text{C}_4\text{D}_8\text{O}$ 9:1) δ (ppm): 2.57 (s, 6H, 1,7-Me-Pn*), 2.52 (s, 6H, 3,5-Me-Pn*), 2.08 (s, 6H, 2,6-Me-Pn*), -0.94 (m, 2H, Ti-H), -1.94 (m, 2H, Ti-H), -4.36 (m, 1H, Ti-H). $^{13}\text{C}\{^1\text{H}\}$ NMR (100 MHz, 298 K, $\text{C}_4\text{D}_8\text{O}$) δ (ppm): 122.2 (4-Pn*), 121.6 (2,6-Pn*), 119.9 (8-Pn*), 109.7 (1,7-Pn*), 108.6 (3,5-Pn*), 14.7 (3,5-Me-Pn*), 14.4 (1,7-Me-Pn*), 10.9 (2,6-Me-Pn*). ^7Li NMR (156 MHz, 298 K, $\text{C}_4\text{D}_8\text{O}$) δ (ppm): 1.22. FTIR (KBr disc, cm^{-1}): 2977 (s), 2952 (s), 2885 (br, s), 1507 (br, s), 1454 (br, s), 1291 (br, s), 1052 (m), 1024 (m), 896 (w). Anal calcd (found) for $\text{C}_{31.6}\text{H}_{48.2}\text{LiTi}_2\text{O}$: C, 69.62 (68.90); H, 8.85 (8.80) – based on $x = 0.9$.

$\text{Pn}^*_2\text{Ti}_2(\mu_2\text{-D})_5\text{Li.thf}_x$. Synthesized using an analogous route to $\text{Pn}^*_2\text{Ti}_2(\mu_2\text{-H})_5\text{Li.thf}_x$ with LiAlD_4 ($[\text{Pn}^*\text{TiCl}(\mu\text{-Cl})_2$ (0.250 g, 0.410 mmol), LiAlD_4 (0.861 g, 2.05 mmol)). $\text{Pn}^*_2\text{Ti}_2(\mu_2\text{-D})_5\text{Li.thf}_x$ was isolated in 64% yield as a yellow crystalline solid (0.146 g, 0.262 mmol, x was determined to be 0.96 by ^1H NMR spectroscopy). ^1H NMR (400 MHz, 298 K, $\text{C}_6\text{D}_6/\text{C}_4\text{D}_8\text{O}$ 9:1) δ (ppm): 2.51 (s, 6H, 1,7-Me-Pn*), 2.46 (s, 6H, 3,5-Me-Pn*), 2.02 (s, 6H, 2,6-Me-Pn*). $^{13}\text{C}\{^1\text{H}\}$ NMR (100 MHz, 298 K, $\text{C}_6\text{D}_6/\text{C}_4\text{D}_8\text{O}$ 9:1) δ (ppm): 122.8 (4-Pn*), 122.2 (2,6-Pn*), 119.4 (8-Pn*), 110.1 (1,7-Pn*), 108.1 (3,5-Pn*), 14.2 (3,5-Me-Pn*), 13.7 (1,7-Me-Pn*), 10.4 (2,6-Me-Pn*). ^2H NMR (76.7 MHz, 298 K, $\text{C}_6\text{D}_6/\text{C}_4\text{D}_8\text{O}$ 9:1) δ (ppm): -1.06 (2D, Ti-D), -2.12 (2D, Ti-D), -4.49 (1D, Ti-D). ^7Li NMR

(156 MHz, 298 K, C₆D₆/C₄D₈O 9:1) δ (ppm): 1.39. FTIR (KBr disc, cm⁻¹): 2977 (s), 2952 (s), 2887 (br, s), 1452 (br, m), 1377 (m), 1099 (br, m), 1052 (s), 941 (s), 805 (w). Anal calcd (found) for C₃₂H₄₄D₃LiTi₂O: C, 68.95 (67.83); H, 9.76 (9.42).

[Pn*₂Zr₂(μ_2 -H)₄(μ_3 -H)Li.thf]₂. [ZrPn*(μ -Cl)_{3/2}]₂(μ -Cl)₂Li.thf₂ (0.200 g, 0.226 mmol) and LiAlH₄ (0.430 g, 1.13 mmol) were dissolved in thf (10 mL) and stirred at room temperature for 4 days. An aliquot was taken, and if necessary, further LiAlH₄ was added and stirred for 36 h. Once complete, the volatiles were removed under vacuum and the gray solid was extracted with benzene (4 × 7 mL) and filtered through celite. The combined extracts were concentrated to ca. 10 mL, and the mixture was lyophilized under dynamic vacuum to give a flocculent pale yellow solid. This was redissolved in a minimum volume of thf (3 × 4 mL) and filtered a second time through celite. The volatiles were removed under vacuum, slurried in benzene (5 mL), and lyophilized under dynamic vacuum, yielding [Pn*₂Zr₂(μ_2 -H)₄(μ_3 -H)Li.thf]₂ in 34% yield (46 mg, 0.038 mmol, α = 0.5, determined by ¹H NMR spectroscopy). Single crystals of [Pn*₂Zr₂(μ_2 -H)₄(μ_3 -H)Li.thf]₂ suitable for an X-ray diffraction study were grown by slow evaporation of a thf solution. ¹H NMR (400 MHz, 298 K, C₄D₈O) δ (ppm): 2.30 (s, 6H, 1,7-Me-Pn*), 2.28 (s, 6H, 3,5-Me-Pn*), 2.03 (s, 6H, 2,6-Me-Pn*), 1.67 (s, 2H, Zr-H), 1.51 (s, 2H Zr-H), -0.55 (s, 1H, Zr-H). ¹H NMR (400 MHz, 298 K, C₆D₆/C₄D₈O 8:2) δ (ppm): 2.54 (s, 6H, 1,7-Me-Pn*), 2.51 (s, 6H, 3,5-Me-Pn*), 2.14 (s, 6H, 2,6-Me-Pn*), 1.89 (s, 2H, Zr-H), 1.73 (s, 2H Zr-H), -0.31 (s, 1H, Zr-H). ¹³C{¹H} NMR (100 MHz, 298 K, C₄D₈O) δ (ppm): 122.0120.0 (4,8-Pn* could not be distinguished by heteronuclear multiple bond correlation (HMBC)), 125.0, 105.2, 104.7 (1,2,3,5,7-Pn*, could not be distinguished by HMBC), 13.6 (3,5-Me-Pn*), 13.3 (1,7-Me-Pn*), 10.7 (2,6-Me-Pn*). FTIR (KBr disc, cm⁻¹): 2976 (s), 2955 (s), 2905 (s), 2863 (s), 1451 (m), 1380 (m), 1260 (s), 1099 (w), 1046 (w), 1028 (w). Anal calcd (found) for C₆₄H₉₈Li₂O₂Zr₄: C, 60.14 (61.90); H, 7.73 (7.88) – based on α = 1.

[Pn*₂Zr₂(μ_2 -D)₄(μ_3 -D)Li.thf]₂. Synthesized by an analogous route to [Pn*₂Zr₂(μ_2 -H)₄(μ_3 -H)Li.thf]₂ ([ZrPn*(μ -Cl)_{3/2}]₂(μ -Cl)₂Li.thf₂ (0.200 g, 0.226 mmol), LiAlD₄ (0.475 g, 1.13 mmol)). [Pn*₂Zr₂(μ_2 -D)₄(μ_3 -D)Li.thf]₂ was isolated in 41% yield (0.058 g, 0.046 mmol, α = 0.8, determined by ¹H NMR spectroscopy). ¹H NMR (400 MHz, 298 K, C₆D₆/C₄D₈O 8:2) δ (ppm): 2.51 (s, 6H, 1,7-Me-Pn*), 2.49 (s, 6H, 3,5-Me-Pn*), 2.13 (s, 6H, 2,6-Me-Pn*). ¹³C{¹H} NMR (100 MHz, 298 K, C₆D₆/C₄D₈O 8:2) δ (ppm): 122.7, 120.2 (4,8-Pn* could not be distinguished by HMBC), 125.4, 104.9, 104.1 (1,2,3,5,7-Pn*, could not be distinguished by HMBC), 14.0 (3,5-Me-Pn*), 13.7 (1,7-Me-Pn*), 11.1 (2,6-Me-Pn*). ²D NMR (76.7 MHz, 298 K, C₆D₆/C₄D₈O 8:2) δ (ppm): 1.77 (Zr-D), 1.58 (Zr-D), -0.41 (Zr-D). FTIR (KBr disc, cm⁻¹): 2975 (s), 2954 (s), 2905 (s), 2861 (s), 1454 (m), 1382 (m), 1049 (m), 1020 (br, m), 915 (br, s), 812 (m).

Pn*Ti(CH₂SiMe₃)₂. A Youngs tap side arm Schlenk was charged with [Pn*TiCl](μ -Cl)₂ (0.400 g, 0.656 mmol) and NaCH₂SiMe₃ (0.318 g, 2.885 mmol) to which pentane (40 mL) was added and allowed to stir for 16 h. The resulting purple suspension was filtered through celite on a sintered glass frit and eluted with pentane until colorless. The solution was reduced to minimum volume and cooled to -78 °C, which yielded a deep purple microcrystalline solid, which was collected in two crops in 72% total yield. ¹H NMR (300 MHz, 298 K, C₆D₆) δ (ppm): 1.87 (s, 12H, 1,3,5,7-Me-Pn*), 1.84 (s, 6H, 2,6-Me-Pn*), 0.25 (s, 18H, SiMe₃), -0.15 (s, 4H, Ti-CH₂). ¹³C{¹H} NMR (75 MHz, 298 K, C₆D₆) δ (ppm): 137.0 (4,8-Pn*), 130.1 (2,6-Pn*), 116.9 (1,3,5,7-Pn*), 56.4 (t, ¹J_{C-H} = 105.3, TiCH₂), 13.2 (q, ¹J_{C-H} = 126.8, 1,3,5,7-Me-Pn*), 11.6 (q, ¹J_{C-H} = 127.2, 2,6-Me-Pn*), 4.0 (q, ¹J_{C-H} = 116.1, SiMe₃). Anal calcd (found) for C₂₂H₄₀TiSi₂: C, 64.47 (64.49); H, 9.87 (9.67).

Pn*₃Ti₃(μ_2 -H)₃(μ_3 -H). Pn*Ti(CH₂SiMe₃)₂ (0.150 g, 0.367 mmol) was dissolved in toluene (5 mL) and freeze-pump-thaw degassed. H₂ gas (1 bar overpressure) was added at room temperature, leading to a slow color change from purple to green-black. The solution was stirred for 48 h before the volatiles were removed under dynamic vacuum overnight. Pn*₃Ti₃(μ_2 -H)₃(μ_3 -H) was isolated as a pure black

microcrystalline solid in 71% yield (0.061 mg, 0.086 mmol). ¹H NMR (400 MHz, 298 K, C₆D₆) δ (ppm): 2.30 (s, 12H, 1,3,5,7-Me-Pn*), 2.15 (s, 6H, 2,6-Me-Pn*), -2.91 (s, 4H, Ti-H). ¹³C{¹H} NMR (100 MHz, 298 K, C₆D₆) δ (ppm): 123.1 (4,8-Pn*), 122.0, 112.4 (1,3,5,7-Pn*), 15.5 (1,3,5,7-Me-Pn*), 12.1 (2,6-Me-Pn*). FTIR (KBr disc, cm⁻¹): 2991 (w), 1959 (m), 2906 (s), 2857 (s), 1443 (br, s), 1373 (s), 1310 (w), 1042 (m), 1021 (s), 947 (m), 800 (m). Anal calcd (found) for C₄₂H₅₈Ti₃: C, 71.40 (71.29); H, 8.27 (8.37).

Pn*₃Ti₃(μ_2 -D)₃(μ_3 -D). Pn*Ti(CH₂SiMe₃)₂ (0.150 g, 0.367 mmol) was dissolved in toluene (5 mL) and freeze-pump-thaw degassed. D₂ gas (1 bar overpressure) was added at room temperature, leading to a slow color change from purple to green-black. The solution was stirred for 48 h before the volatiles were removed under dynamic vacuum overnight. Pn*₃Ti₃(μ_2 -D)₃(μ_3 -D) was isolated as a pure black microcrystalline solid in 65% yield (0.057 g, 0.080 mmol). ¹H NMR (400 MHz, 298 K, C₆D₆) δ (ppm): 2.30 (s, 12H, 1,3,5,7-Me-Pn*), 2.15 (s, 6H, 2,6-Me-Pn*). ¹³C{¹H} NMR (100 MHz, 298 K, C₆D₆) δ (ppm): 123.8 (4,8-Pn*), 122.1, 112.2 (1,3,5,7-Pn*), 15.5 (1,3,5,7-Me-Pn*), 12.3 (2,6-Me-Pn*). ²D NMR (76.7 MHz, 298 K, C₆D₆) δ (ppm): -3.1 ppm (Ti-D). Anal calcd (found) for C₄₂H₅₄D₄Ti₃: C, 71.00 (71.35); H, 8.79 (8.92).

ASSOCIATED CONTENT

Supporting Information

The Supporting Information is available free of charge at <https://pubs.acs.org/doi/10.1021/acs.inorgchem.2c01267>.

Additional experimental details, representative NMR spectra, crystallographic collection and refinement details, and computational details (PDF)

Accession Codes

CCDC 2164608–2164612 contain the supplementary crystallographic data for this paper. These data can be obtained free of charge via www.ccdc.cam.ac.uk/data_request/cif, or by emailing data_request@ccdc.cam.ac.uk, or by contacting The Cambridge Crystallographic Data Centre, 12 Union Road, Cambridge CB2 1EZ, UK; fax: +44 1223 336033.

AUTHOR INFORMATION

Corresponding Authors

Jennifer C. Green – Department of Chemistry, Chemistry Research Laboratory, Oxford OX1 3TA, U.K.;

Email: jennifer.green@chem.ox.ac.uk

Dermot O'Hare – Department of Chemistry, Chemistry Research Laboratory, Oxford OX1 3TA, U.K.; orcid.org/0000-0001-8054-8751; Email: dermot.ohare@chem.ox.ac.uk

Authors

Duncan A. X. Fraser – Department of Chemistry, Chemistry Research Laboratory, Oxford OX1 3TA, U.K.

Zoë R. Turner – Department of Chemistry, Chemistry Research Laboratory, Oxford OX1 3TA, U.K.; orcid.org/0000-0003-2044-9203

Robert T. Cooper – Department of Chemistry, Chemistry Research Laboratory, Oxford OX1 3TA, U.K.

Jean-Charles Buffet – Department of Chemistry, Chemistry Research Laboratory, Oxford OX1 3TA, U.K.; orcid.org/0000-0003-2062-9546

Complete contact information is available at:

<https://pubs.acs.org/doi/10.1021/acs.inorgchem.2c01267>

Author Contributions

The manuscript was written through contributions of all authors. All authors have given approval to the final version of the manuscript.

Funding

This work was funded by SCG Chemicals Co. Ltd. (Thailand).

Notes

The authors declare no competing financial interest.

ACKNOWLEDGMENTS

D.A.X.F., Z.R.T., J.-C.B., and D.O.H. gratefully acknowledge funding from SCG Chemicals Co. Ltd. for this work. The authors thank CHEMICAL Crystallography (Oxford) for helpful guidance and use of the diffractometers.

REFERENCES

- (1) (a) Yagupsky, M.; Wilkinson, G. Further studies on hydridocarbonyltris(triphenylphosphine)rhodium(I). Part II. Isomerisation of n-pentenes and hex-1-ene. *J. Chem. Soc. A* **1970**, 941–944. (b) Ager, D. J.; de Vries, A. H. M.; de Vries, J. G. Asymmetric homogeneous hydrogenations at scale. *Chem. Soc. Rev.* **2012**, *41*, 3340–3380. (c) Johnson, N. B.; Lennon, I. C.; Moran, P. H.; Ramsden, J. A. Industrial-Scale Synthesis and Applications of Asymmetric Hydrogenation Catalysts. *Acc. Chem. Res.* **2007**, *40*, 1291–1299. (d) Shultz, C. S.; Krska, S. W. Unlocking the Potential of Asymmetric Hydrogenation at Merck. *Acc. Chem. Res.* **2007**, *40*, 1320–1326. (e) Blaser, H.-U.; Pugin, B.; Spindler, F.; Thommen, M. From a Chiral Switch to a Ligand Portfolio for Asymmetric Catalysis. *Acc. Chem. Res.* **2007**, *40*, 1240–1250. (f) Pospech, J.; Fleischer, I.; Franke, R.; Buchholz, S.; Beller, M. Alternative Metals for Homogeneous Catalyzed Hydroformylation Reactions. *Angew. Chem., Int. Ed.* **2013**, *52*, 2852–2872.
- (2) (a) McGrady, G. S.; Guilera, G. The multifarious world of transition metal hydrides. *Chem. Soc. Rev.* **2003**, *32*, 383–392. (b) Belkova, N. V.; Epstein, L. M.; Filippov, O. A.; Shubina, E. S. Hydrogen and Dihydrogen Bonds in the Reactions of Metal Hydrides. *Chem. Rev.* **2016**, *116*, 8545–8587. (c) Wiedner, E. S.; Chambers, M. B.; Pitman, C. L.; Bullock, R. M.; Miller, A. J. M.; Appel, A. M. Thermodynamic Hydricity of Transition Metal Hydrides. *Chem. Rev.* **2016**, *116*, 8655–8692. (d) Maity, A.; Teets, T. S. Main Group Lewis Acid-Mediated Transformations of Transition-Metal Hydride Complexes. *Chem. Rev.* **2016**, *116*, 8873–8911.
- (3) (a) Bauer, I.; Knölker, H.-J. Iron Catalysis in Organic Synthesis. *Chem. Rev.* **2015**, *115*, 3170–3387. (b) Chirik, P. J. Iron- and Cobalt-Catalyzed Alkene Hydrogenation: Catalysis with Both Redox-Active and Strong Field Ligands. *Acc. Chem. Res.* **2015**, *48*, 1687–1695. (c) Li, Y.-N.; Ma, R.; He, L.-N.; Diao, Z.-F. Homogeneous hydrogenation of carbon dioxide to methanol. *Catal. Sci. Technol.* **2014**, *4*, 1498–1512. (d) Van Leeuwen, P. W., *Homogeneous catalysis: understanding the art*; Springer Science & Business Media, 2006. (e) Parshall, G. W.; Ittel, S. D. *Homogeneous catalysis*; Wiley, 1992. (f) Robinson, S. J. C.; Heinekey, D. M. Hydride & dihydrogen complexes of earth abundant metals: structure, reactivity, and applications to catalysis. *Chem. Commun.* **2017**, *53*, 669–676.
- (4) (a) Jones, S. B.; Petersen, J. L. Preparation and structural characterization of early-transition-metal hydrides. [(eta-5-C₅H₄CH₃)₂ZrH(mu-H)]₂, a binuclear zirconium hydride complex. *Inorg. Chem.* **1981**, *20*, 2889–2894. (b) Hoskin, A. J.; Stephan, D. W. Early transition metal hydride complexes: synthesis and reactivity. *Coord. Chem. Rev.* **2002**, *233-234*, 107–129. (c) Larssonneur, A. M.; Choukroun, R.; Jaud, J. Synthesis, characterization, and chemical reactivity of zirconium dihydride [(C₅H₄R)₂Zr(mu-H)H]₂ (R = SiMe₃, CMe₃). H/D exchange reactions of anionic species [(C₅H₄R)₂ZrH₂]⁻. X-ray crystal structure of [(C₅H₄SiMe₃)₂Zr(mu-H)H]₂. *Organometallics* **1993**, *12*, 3216–3224.
- (5) Harrod, J. F. Catalysis of reactions of Si-H by titanocene and its derivatives. *Coord. Chem. Rev.* **2000**, *206-207*, 493–531.
- (6) (a) Resconi, L.; Cavallo, L.; Fait, A.; Piemontesi, F. Selectivity in Propene Polymerization with Metallocene Catalysts. *Chem. Rev.* **2000**, *100*, 1253–1346. (b) Carr, A. G.; Dawson, D. M.; Thornton-Pett, M.; Bochmann, M. Cationic Zirconocene Hydrides: A New Type of Highly Effective Initiators for Carbocationic Polymerizations. *Organometallics* **1999**, *18*, 2933–2935. (c) Tilley, T. D. The coordination polymerization of silanes to polysilanes by a “sigma-bond metathesis” mechanism. Implications for linear chain growth. *Acc. Chem. Res.* **1993**, *26*, 22–29.
- (7) (a) Wolczanski, P. T.; Bercaw, J. E. Mechanisms of carbon monoxide reduction with zirconium hydrides. *Acc. Chem. Res.* **1980**, *13*, 121–127. (b) Moore, E. J.; Straus, D. A.; Armantrout, J.; Santarsiero, B. D.; Grubbs, R. H.; Bercaw, J. E. Synthesis and structure of ketene complexes of permethylzirconocene and their hydrogenation to zirconium enolate hydrides. *J. Am. Chem. Soc.* **1983**, *105*, 2068–2070. (c) Kropp, K.; Skibbe, V.; Erker, G.; Krueger, C. Fischer-Tropsch intermediates: tris[(eta-2-formaldehyde)zirconocene] from the carbonylation of a zirconium hydride. *J. Am. Chem. Soc.* **1983**, *105*, 3353–3354. (d) Gambarotta, S.; Floriani, C.; Chiesi-Villa, A.; Guastini, C. Genesis, bonding mode and reaction with carbon monoxide of an oxymethylene unit bridging two metal atoms. *J. Am. Chem. Soc.* **1983**, *105*, 1690–1691. (e) Berno, P.; Floriani, C.; Chiesi-Villa, A.; Guastini, C. Fourteen electron monoalkyl and monohydrido derivatives of cyclooctatetraenzirconium: reduction of carbon monoxide to formaldehyde. *J. Chem. Soc., Chem. Commun.* **1991**, *2*, 109–110.
- (8) (a) Fryzuk, M. D.; Love, J. B.; Rettig, S. J.; Young, V. G. Transformation of coordinated dinitrogen by reaction with dihydrogen and primary silanes. *Science* **1997**, *275*, 1445–1447. (b) Pool, J. A.; Lobkovsky, E.; Chirik, P. J. Hydrogenation and cleavage of dinitrogen to ammonia with a zirconium complex. *Nature* **2004**, *427*, 527–530. (c) Ballmann, J.; Munhá, R. F.; Fryzuk, M. D. The hydride route to the preparation of dinitrogen complexes. *Chem. Commun.* **2010**, *46*, 1013–1025.
- (9) (a) Kautzner, B.; Wailes, P. C.; Weigold, H. Hydrides of bis(cyclopentadienyl)zirconium. *J. Chem. Soc. D* **1969**, *19*, 1105a–1105a. (b) Schwartz, J.; Labinger, J. A. Hydrozirconation: A New Transition Metal Reagent for Organic. *Synthesis* **1976**, *15*, 333–340. (c) Pinheiro, D. L. J.; de Castro, P. P.; Amarante, G. W. Recent Developments and Synthetic Applications of Nucleophilic Zirconocene Complexes from Schwartz's Reagent. **2018**, *2018* (35), 4828–4844, DOI: 10.1002/ejoc.201800852. (d) Wiąclaw, M. M.; Stecko, S. Hydrozirconation of C=X Functionalities with Schwartz's Reagent. *Eur. J. Org. Chem.* **2018**, *2018*, 6601–6623. (e) Kehner, R. A.; Hewitt, M. C.; Bayeh-Romero, L. Expanding Zirconocene Hydride Catalysis: In Situ Generation and Turnover of ZrH Catalysts Enabling Catalytic Carbonyl Reductions. *ACS Catal.* **2022**, *12*, 1758–1763.
- (10) (a) Kang, X.; Luo, G.; Luo, L.; Hu, S.; Luo, Y.; Hou, Z. Mechanistic Insights into Ring Cleavage and Contraction of Benzene over a Titanium Hydride Cluster. *J. Am. Chem. Soc.* **2016**, *138*, 11550–11559. (b) Hu, S.; Shima, T.; Hou, Z. Carbon-carbon bond cleavage and rearrangement of benzene by a trinuclear titanium hydride. *Nature* **2014**, *512*, 413–415. (c) Shima, T.; Hu, S.; Luo, G.; Kang, X.; Luo, Y.; Hou, Z. Dinitrogen Cleavage and Hydrogenation by a Trinuclear Titanium Polyhydride Complex. *Science* **2013**, *340*, 1549–1552. (d) Hu, S.; Shima, T.; Luo, Y.; Hou, Z. Tetranuclear Zirconium and Hafnium Polyhydride Complexes Composed of the “CpMH₂” Units. *Organometallics* **2013**, *32*, 2145–2151. (e) Shima, T.; Luo, G.; Hu, S.; Luo, Y.; Hou, Z. Experimental and Computational Studies of Dinitrogen Activation and Hydrogenation at a Tetranuclear Titanium Imide/Hydride Framework. *J. Am. Chem. Soc.* **2019**, *141*, 2713–2720. (f) Liu, F.-C.; Chu, Y.-J.; Yang, C.-C.; Lee, G.-H.; Peng, S.-M. Syntheses and Structures of Zirconium Tetranuclear Polyhydrides. *Organometallics* **2010**, *29*, 2685–2692.
- (11) (a) Kulinna, H.; Spaniol, T. P.; Maron, L.; Okuda, J. Cationic Zirconium Hydrides Supported by an NNNN-Type Macrocyclic Ligand: Synthesis, Structure, and Reactivity. *Inorg. Chem.* **2012**, *51*, 12462–12472. (b) Munhá, R. F.; Ballmann, J.; Veiros, L. F.; Patrick, B. O.; Fryzuk, M. D.; Martins, A. M. Dinuclear Cationic Zirconium

- Hydrides Stabilized by the N,N-Dibenzylcyclam Ancillary Ligand. *Organometallics* **2012**, *31*, 4937–4940. (c) Kulinna, H.; Spaniol, T. P.; Okuda, J. Neutral and Cationic Zirconium Hydrides Supported by a Dianionic (NNNN)-Type Macrocyclic Ligand. *Organometallics* **2015**, *34*, 2160–2164. (d) Nakanishi, Y.; Ishida, Y.; Kawaguchi, H. Zirconium Hydride Complex Supported by a Tetradentate Carbon-Centered Tripodal Tris(aryloxy) Ligand: Synthesis, Structure, and Reactivity. *Inorg. Chem.* **2016**, *55*, 3967–3973. (e) Fryzuk, M. D.; Corkin, J. R.; Patrick, B. O. Reduction of hafnium(IV) complexes in the presence of molecular nitrogen: Attempts to form dinitrogen complexes of the heaviest group 4 element. *Can. J. Chem.* **2003**, *81*, 1376–1387.
- (12) (a) Manriquez, J. M.; McAlister, D. R.; Sanner, R. D.; Bercaw, J. E. Reduction of carbon monoxide promoted by alkyl and hydride derivatives of permethylzirconocene. *J. Am. Chem. Soc.* **1978**, *100*, 2716–2724. (b) Bercaw, J. E.; Marvich, R. H.; Bell, L. G.; Brintzinger, H. H. Titanocene as an intermediate in reactions involving molecular hydrogen and nitrogen. *J. Am. Chem. Soc.* **1972**, *94*, 1219–1238.
- (13) (a) Curtis, C. J.; Haltiwanger, R. C. Preparation of dinuclear zirconium hydride complexes containing the fulvalene ligand and their reactions with carbon monoxide. *Organometallics* **1991**, *10*, 3220–3226. (b) Chirik, P. J.; Day, M. W.; Bercaw, J. E. Preparation and Characterization of Monomeric and Dimeric Group IV Metallocene Dihydrides Having Alkyl-Substituted Cyclopentadienyl Ligands. *Organometallics* **1999**, *18*, 1873–1881. (c) Guo, Z. Y.; Bradley, P. K.; Jordan, R. F. THF ring-opening and hydrogen/deuterium exchange reactions of (C₅H₄Me)₂Zr(H)(THF)⁺. Evidence for hydrogenolysis of zirconium-cyclopentadiene bonds. *Organometallics* **1992**, *11*, 2690–2693. (d) Kurogi, T.; Kamitani, M.; Carroll, P. J.; Mindiola, D. J. Polyhydrides of Sc, Zr and Hf and Their Proposed Formation. *Isr. J. Chem.* **2017**, *57*, 999–1009.
- (14) (a) Grossman, R. B.; Doyle, R. A.; Buchwald, S. L. Syntheses of [ethylene-1,2-bis(eta.5-4,5,6,7-tetrahydro-1-indenyl)]zirconium and -hafnium hydride complexes. Improved syntheses of the corresponding dichlorides. *Organometallics* **1991**, *10*, 1501–1505. (b) Wielstra, Y.; Gambarotta, S.; Spek, A. L. Monocyclopentadienyl zirconium and hafnium alkyls: synthesis, hydrogen-transfer reactions and catalytic features in the reactivity with alpha-olefins. The x-ray structure of CpZr(eta.4-butadiene)(DMPE)Cl [DMPE = 1,2-bis(dimethylphosphino)ethane]. *Organometallics* **1990**, *9*, 572–577.
- (15) Heiden, Z. M.; Lathem, A. P. Establishing the Hydride Donor Abilities of Main Group Hydrides. *Organometallics* **2015**, *34*, 1818–1827.
- (16) (a) Pool, J. A.; Bradley, C. A.; Chirik, P. J. A Convenient Method for the Synthesis of Zirconocene Hydrido Chloride, Isobutyl Hydride, and Dihydride Complexes Using tert-Butyl Lithium. *Organometallics* **2002**, *21*, 1271–1277. (b) Yan, K.; Ellern, A.; Sadow, A. D. Nonclassical beta-Hydrogen Elimination of Hydrosilazido Zirconium Compounds via Direct Hydrogen Transfer. *J. Am. Chem. Soc.* **2012**, *134*, 9154–9156. (c) Brintzinger, H. H.; Fischer, D.; Müllhaupt, R.; Rieger, B.; Waymouth, R. M. Stereospecific Olefin Polymerization with Chiral Metallocene Catalysts. *Angew. Chem., Int. Ed. Engl.* **1995**, *34*, 1143–1170. (d) Coates, G. W. Precise Control of Polyolefin Stereochemistry Using Single-Site Metal Catalysts. *Chem. Rev.* **2000**, *100*, 1223–1252.
- (17) (a) Bercaw, J. E. Bis(pentamethylcyclopentadienyl)titanium(II) and its complexes with molecular nitrogen. *J. Am. Chem. Soc.* **1974**, *96*, 5087–5095. (b) Brintzinger, H.; Bercaw, J. E. Bis(pentamethylcyclopentadienyl)titanium(II). Isolation and reactions with hydrogen, nitrogen, and carbon monoxide. *J. Am. Chem. Soc.* **1971**, *93*, 2045–2046. (c) Pinkas, J.; Gyepes, R.; Císarová, I.; Kubišta, J.; Horáček, M.; Mach, K. Decamethyltitanocene hydride intermediates in the hydrogenation of the corresponding titanocene-(eta²-ethene) or (eta²-alkyne) complexes and the effects of bulkier auxiliary ligands. *Dalton Trans.* **2017**, *46*, 8229–8244.
- (18) (a) Sizov, A. I.; Zvukova, T. M.; Bel'sky, V. K.; Bulychev, B. M. Activation of bicyclopentadienyl hydride complexes of titanium and aluminum by NH- and OH-acids in the reactions of hydrogenation of olefins. Crystal and molecular structures of {[(eta⁵-Cp)₂Ti(mu-H)2AlH]mu-N(C₂H₄)₄O}}₂ and [(eta⁵-Cp)₂Ti(mu-H)(2AlH)2(mu-OC₂H₄OMe)][(mu¹:mu⁵-C₅H₄)Ti(mu⁵-Cp)(mu-H)]₂*. *Russ. Chem. Bull.* **1998**, *47*, 1186–1192. (b) Bulichev, B. M.; Evdokimova, E. V.; Sizov, A. I.; Soloveichik, G. L. Isomerization of olefins on hydride-halide compounds of titanium and aluminum of composition LmTiH₂AlX'. The role of the cocatalyst and the geometry of the ligand environment of the titanium atom in catalytic hydrogen transfer. *J. Organomet. Chem.* **1982**, *239*, 313–320. (c) Bel'sky, V. K.; Sizov, A. I.; Bulychev, B. M.; Soloveichik, G. L. Structural chemistry of titanium and aluminum bimetallic hydride complexes: IV. Molecular structures and catalytic properties of {[(eta⁵-C₅(CH₃)₅)₂Ti(mu²-H)-2Al(H)(mu²-H)]₂ and [eta⁵-C₅(CH₃)₅)₂Ti(mu²-H)2Al(H)(mu²-H)2Ti[eta⁵-C₅(CH₃)₅]₂}. *J. Organomet. Chem.* **1985**, *280*, 67–80.
- (19) (a) Mach, K.; Varga, V.; Hanuš, V. Formation of fulvene and dimethylenecyclopentenyl titanium complexes from bis(eta⁵-tetramethylcyclopentadienyl)titanium(IV) precursors. *J. Organomet. Chem.* **1991**, *415*, 87–95. (b) Troyanov, S. I.; Mach, K.; Varga, V. Synthesis and structure of a novel mu-dimethyldimethylenecyclopentenyl bis(mu-hydrido) mixed-valence titanium(III)/titanium(II) compound. *Organometallics* **1993**, *12*, 3387–3389.
- (20) Emsley, J.; Ed. *The Elements*, 3rd ed.; Oxford Univ Press, 1996; p 286
- (21) Etkin, N.; Hoskin, A. J.; Stephan, D. W. The Anionic Zirconocene Trihydride: [Cp*₂ZrH₃]. *J. Am. Chem. Soc.* **1997**, *119*, 11420–11424.
- (22) Wailes, P. C.; Weigold, H. Hydrido complexes of zirconium I. Preparation. *J. Organomet. Chem.* **1970**, *24*, 405–411.
- (23) Khan, K.; Raston, C. L.; McGrady, J. E.; Skelton, B. W.; White, A. H. Hydride-Bridged Heterobimetallic Complexes of Zirconium and Aluminum. *Organometallics* **1997**, *16*, 3252–3254.
- (24) Sizov, A. I.; Zvukova, T. M.; Khvostov, A. V.; Belsky, V. K.; Stash, A. I.; Bulychev, B. M. Transition metal-catalyzed reduction of ZrIV in Cp₂ZrX₂—LiAlH₄ and Cp₂ZrX₂—AlH₃ (X=Cl, Br, I) systems: structural study of resulting zirconocene(III) aluminum hydride complexes. *J. Organomet. Chem.* **2003**, *681*, 167–173.
- (25) Chirik, P. J.; Henling, L. M.; Bercaw, J. E. Synthesis of Singly and Doubly Bridged ansa-Zirconocene Hydrides. Formation of an Unusual Mixed Valence Trimeric Hydride by Reaction of H₂ with {(Me₂Si)₂(eta⁵-C₅H₃)₂}Zr(CH₃)₂ and Generation of a Dinitrogen Complex by Reaction of N₂ with a Zirconocene Dihydride. *Organometallics* **2001**, *20*, 534–544.
- (26) Cuenca, T.; Galakhov, M.; Royo, E.; Royo, P. Hydride derivatives of Group 4 metals with the ansa-(SiMe₂)₂(eta⁵-C₅H₃)₂ ligand. *J. Organomet. Chem.* **1996**, *515*, 33–36.
- (27) (a) Green, J. C.; Green, M. L. H.; Prout, C. K. A bonding model for bent bis(pi-cyclopentadienyl) metal compounds. *J. Chem. Soc., Chem. Commun.* **1972**, *7*, 421–422. (b) Petersen, J. L.; Dahl, L. F. Synthesis and structural characterization by x-ray diffraction and EPR single-crystal techniques of (dichloro)bis(eta.5-methylcyclopentadienyl)vanadium and (dichloro)bis(eta.5-methylcyclopentadienyl)titanium. Spatial distribution of the unpaired electron in a V(eta.5-C₅H₅)₂L₂-type complex. *J. Am. Chem. Soc.* **1975**, *97*, 6422–6433. (c) Long, N. J. *Metallocenes - An Introduction to Sandwich Complexes*; Blackwell Scientific Publications, 1998; (d) Green, J. C. Bent metallocenes revisited. *Chem. Soc. Rev.* **1998**, *27*, 263–272.
- (28) Green, J. C.; Jackson, S. E.; Higginson, B. Photoelectron studies of some bent bis(eta-cyclopentadienyl)metal complexes. Part I. Some eighteen-electron systems with hydride, alkyl, olefin, allyl, and carbonyl ligands. *J. Chem. Soc., Dalton Trans.* **1975**, *5*, 403–409.
- (29) Wailes, P. C. Vanadium, Niobium and Tantalum: Annual survey covering the year 1975. *J. Organomet. Chem.* **1976**, *119*, 243–259.
- (30) (a) Becke, A. D. Density functional calculations of molecular bond energies. *J. Chem. Phys.* **1986**, *84*, 4524–4529. (b) Lee, C.; Yang, W.; Parr, R. G. Development of the Colle-Salvetti correlation-energy formula into a functional of the electron density. *Phys. Rev. B* **1988**, *37*, 785–789. (c) Becke, A. D. Density-functional thermo-

chemistry. III. The role of exact exchange. *J. Chem. Phys.* **1993**, *98*, 5648–5652.

(31) (a) Schäfer, A.; Horn, H.; Ahlrichs, R. Fully optimized contracted Gaussian basis sets for atoms Li to Kr. *J. Chem. Phys.* **1992**, *97*, 2571–2577. (b) Schäfer, A.; Huber, C.; Ahlrichs, R. Fully optimized contracted Gaussian basis sets of triple zeta valence quality for atoms Li to Kr. *J. Chem. Phys.* **1994**, *100*, 5829–5835. (c) Weigend, F.; Ahlrichs, R. Balanced basis sets of split valence, triple zeta valence and quadruple zeta valence quality for H to Rn: Design and assessment of accuracy. *Phys. Chem. Chem. Phys.* **2005**, *7*, 3297–3305.

(32) (a) Mayer, I. Bond order and valence indices: A personal account. *J. Comput. Chem.* **2007**, *28*, 204–221. (b) Bridgeman, A. J.; Cavigliasso, G.; Ireland, L. R.; Rothery, J. The Mayer bond order as a tool in inorganic chemistry. *J. Chem. Soc., Dalton Trans.* **2001**, *14*, 2095–2108.

(33) Cooper, R. T.; Chadwick, F. M.; Ashley, A. E.; O'Hare, D. Synthesis and Characterization of Group 4 Permethylpentalene Dichloride Complexes. *Organometallics* **2013**, *32*, 2228–2233.

(34) te Velde, G.; Bickelhaupt, F. M.; Baerends, E. J.; Fonseca Guerra, C.; van Gisbergen, S. J. A.; Snijders, J. G.; Ziegler, T. Chemistry with ADF. *J. Comput. Chem.* **2001**, *22*, 931–967.

(35) Vosko, S. H.; Wilk, L.; Nusair, M. Accurate spin-dependent electron liquid correlation energies for local spin density calculations: a critical analysis. *Phys. Rev. B* **1980**, *21*, 1200–1211, DOI: [10.1139/p80-159](https://doi.org/10.1139/p80-159).

(36) (a) Becke, A. D. Density-functional exchange-energy approximation with correct asymptotic behavior. *Phys. Rev. A* **1988**, *38*, 3098–3100. (b) Perdew, J. P. Density-functional approximation for the correlation energy of the inhomogeneous electron gas. *Phys. Rev. B* **1986**, *33*, 8822–8824.